Journal of The Electrochemical Society, **154** (2) B139-B146 (2007)
0013-4651/2006/154(2)/B139/8/$20.00 © The Electrochemical Society

Analysis of Cold Start in Polymer Electrolyte Fuel Cells

Leng Mao and Chao-Yang Wang*,z

Electrochemical Engine Center (ECEC) and Department of Mechanical and Nuclear Engineering, The Pennsylvania State University, University Park, Pennsylvania 16802, USA

To enhance cold start capability and survivability of polymer electrolyte fuel cells (PEFCs) at subzero temperatures, a fundamental understanding of the principles involved is required. In this work an analytical model is presented to describe heat balance, ice formation in the catalyst layer, water transport characteristics throughout a fuel cell at very low temperatures, and the ensuing voltage behavior during PEFC cold start. The model is used to elucidate cold start behaviors of a PEFC from −10 and −20°C and to identify key parameters controlling PEFC cold start, such as the initial membrane water content prior to startup and thermal mass of bipolar plates.
 [DOI: 10.1149/1.2402123]

Manuscript submitted August 9, 2006; revised manuscript received September 15, 2006.
Available electronically December 15, 2006.

Cold start capability and survivability of polymer electrolyte fuel cells (PEFCs) in a subzero environment remains a major challenge for automotive applications. Fundamental mechanisms are not fully determined, but it is recognized that product water becomes ice or frost upon startup when the PEFC internal temperature is below freezing. If the local pore volume of the cathode catalyst layer (CL) is insufficient to contain all of the accumulated water before the operating temperature of the cell rises above freezing, the solid ice may plug the CL and stop the electrochemical reaction by starving the reactant gases and reducing the electrochemically active area (ECA).[a] This problem, known to the automotive industry as "cold start," is defined as the startup of a fuel cell from a subzero temperature to normal operation at approximately 80°C. The problem of cold start is important not only due to customers' demand for quick startup, but also because PEFC durability is greatly affected by cold start cycles.

By studying the Nafion 112 membrane and membrane electrode assembly (MEA) through freeze-thaw cycles, McDonald et al. suggested a molecular level rearrangement in the ionomer with the observation of decreases in anisotropy of tensile strength and water swelling.[1] Minimal degradation of CL could be found, however. Cho et al. also studied the changes of MEA characteristics using electrochemical impedance spectroscopy (EIS), cyclic voltammetry (CV), and Brunaer-Emmett-Teller (BET) porosity analysis upon thermal cycling from 80 to −10°C.[2] They found that freezing-thawing leads to severe degradation of the CL, and that much slower degradation can be obtained by applying gas purge or antifreeze solution purge.[3] Note that no net water is produced in freeze-thaw cycles of a PEFC. Oszcipok et al. used CV and BET to investigate MEA degradation in isothermal potentiostatic cold start.[4,5] Cold start cycles are accompanied by water production at subzero temperatures due to power generation. They concluded that ice formation in CL, gas diffusion layer (GDL), and microporous layer (MPL) leads to significant performance loss and particularly to decreasing Pt surface area in the cathode CL through cold start cycling. In addition, they developed a statistical model, based on experimental data, to identify the operating parameters most critical to cold start performance.

Although fundamental principles underlying PEFC cold start and associated MEA degradation remain absent in the literature, many strategies for PEFC cold start have been proposed and patented. These methods can be grossly divided into two groups: thermal management and control of residual water distribution in the cell prior to startup. Thermal management includes cell heating by external sources (e.g., batteries or cooling loops), cell heating by in situ chemical reactions (e.g., injection of a small amount of fuel in the cathode air), and reduction in thermal mass of a cell or stack. For control and minimization of residual water in a PEFC prior to startup, various purge techniques using gas or antifreeze liquids (e.g., water-glycol mixture) have been proposed. Again, without a fundamental knowledge of PEFC cold start and the mechanisms leading to cell shutdown, it is difficult to assess the soundness of the proposed engineering solutions.

Mathematical modeling to enable a basic understanding of PEFC cold start has been scarce. Weisbrod et al. discussed cold start dynamics by developing a lumped stack model of heat requirements and water transients during startup from subfreezing temperatures.[6] A similar layered thermal model was presented by Sundaresan,[7] in which a cell-stack is modeled as a multilayer structure with individual cell components, such as membrane, GDL, and CL, comprising the different layers. Although ice formation and latent heat released during phase change of water are considered in these models, the ice fraction is precalculated simply from the water production rate without considering water transport mechanisms in the fuel cell and the effects of ice formation in the CL. A phenomenological model was developed by Hishinuma et al.[8] in which the water transport and the electrochemical reactions were modeled in one dimension. Water uptake in the membrane initially dried by gas purge, critical to water balance, was, however, not taken into account. The effect of ice formation was not computed from basic principles, but by fitting the experimental polarization curve. Oszcipok et al. used statistical software to analyze their single-cell experiments of isothermal cold start.[4,5] The empirical model was employed to study the effects of air flow rate, initial membrane water content, and degree of MEA degradation. In general, all the published models relied heavily on experimental measurements and did not address the principles of coupled heat and water transport during PEFC cold start.

The objective of the present study is to develop a physical model for PEFC cold start based on the principles of water and heat balance, ice formation in the CL, and its impact on voltage losses. The model is subsequently applied to investigate the effects of operating conditions, such as the startup temperature and initial water content in the membrane, on the performance of PEFC cold start.

Model

Based on the principles of water and heat balance, an analytical model is developed in this section to describe PEFC cold start, especially ice formation and its effects. The specific assumptions made in the present model are (*i*) the fuel cell treated as a lumped system with a uniform temperature; (*ii*) incompressible and ideal gas mixture; (*iii*) isotropic and homogeneous GDL, CL, and membrane; (*iv*) instantaneous and homogeneous ice formation in CL when the water vapor partial pressure in the gas phase exceeds the saturation value,

* Electrochemical Society Active Member.
z E-mail: cxw31@psu.edu
[a] In the present paper ECA is defined as the triple-phase interfacial area rather than that measured by cyclic voltammetry. The latter requires only the Pt/ionomer interface without needing access of gaseous oxygen.

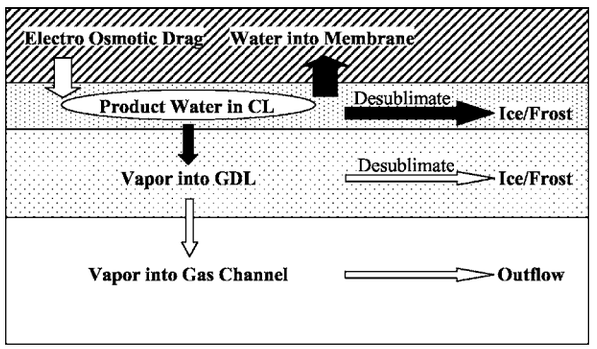

Figure 1. Water transport in fuel cell during cold start.

i.e., instantaneous desublimation; (*v*) negligible ice formation in the GDL due to limited vapor transport at very low startup temperatures of interest (i.e., $\leqslant -10°C$); (*vi*) outflow saturated with water vapor; (*vii*) negligible heat of water absorption in the membrane, and (*viii*) negligible voltage loss due to electronic resistances in CL, GDL, and bipolar plates.

Water balance.— Water flow in the PEFC cathode during cold start is schematically sketched in Fig. 1. To prevent the fuel cell from shutdown by ice formation inside the CL, product water must be diffused into the membrane or transported out into GDL or gas channels, thereby keeping the CL free of ice.

When the water production rate exceeds the removal rate from the CL and the gas phase becomes oversaturated, water will desublimate and form ice in the CL pores. The ice formation rate in the CL (i.e., the water accumulation rate $\dot{n}_{\text{acc}}^{\text{H}_2\text{O}}$) can be estimated by assuming instant desublimation of water accumulated in the CL that cannot be transported into the membrane or GDL. That is

$$\dot{n}_{\text{acc}}^{\text{H}_2\text{O}} = \dot{n}_{\text{CL}}^{\text{H}_2\text{O}} - \dot{n}_{\text{mem}}^{\text{H}_2\text{O}} - \dot{n}_{\text{GDL}}^{\text{H}_2\text{O}} \quad [1]$$

The water generation rate in the cathode CL, the first term on the right-hand side of Eq. 1, can be expressed as the sum of the water production rate from oxygen reduction reaction (ORR) and that dragged from the anode side; namely

$$\dot{n}_{\text{CL}}^{\text{H}_2\text{O}} = \frac{IA}{2F}(1 + n_d) \quad [2]$$

where n_d is the electro-osmotic drag coefficient of water through the membrane. In cold start this drag of water from the anode to cathode is typically balanced by residual water in the anode catalyst layer instead of back-diffusion.

The membrane electrolyte is dehydrated by gas purge prior to cold start, according to the thermodynamic equilibrium relation between the membrane water content (i.e., the number of H_2O molecules per sulfonic group) and water activity of the purge gas.[9,10] Thus, the ionomers serve as a water buffer to uptake product water during cold start, reducing the amount of water subject to ice formation in CL pores. Assuming that the membrane becomes fully hydrated from an initial state of water content λ_0, the maximum amount of water absorbed by the membrane can be expressed as

$$n_{\text{mem}}^{\text{H}_2\text{O}} = \frac{\rho_{\text{dry}}(\lambda_{\text{sat}} - \lambda_0)}{\text{EW}}\delta_{\text{mem}}A \quad [3]$$

where λ_{sat} is the maximum membrane water content when in equilibrium with saturated vapor. For a Nafion 112 membrane with initial water content of 4, this maximum water storage capacity of the membrane is calculated to be 1.7 mg/cm^2. However, for very small water diffusivity characteristic of very low temperatures, the membrane water storage cannot be fully utilized. By assuming the membrane as a semi-infinite slab due to sluggish water diffusion with a uniform water diffusivity, a similarity solution can be used to estimate the actual water uptake rate by the membrane, i.e.,[11]

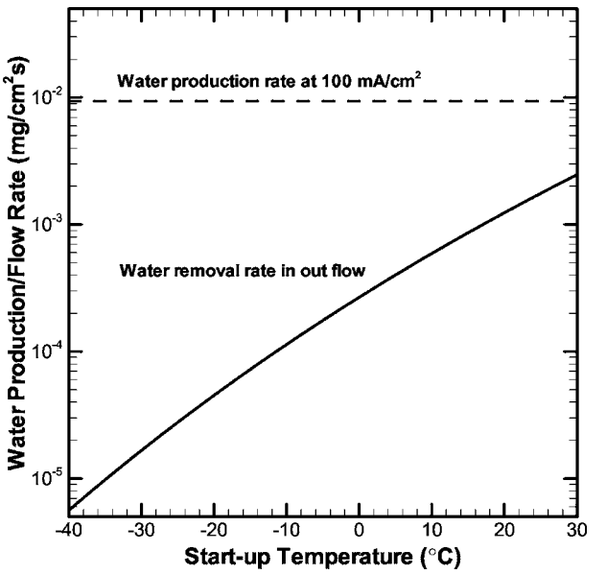

Figure 2. Water removal in the outflow.

$$\dot{n}_{\text{mem}}^{\text{H}_2\text{O}} = \frac{\rho_{\text{dry}}}{\text{EW}}\frac{\sqrt{D_{\text{mem}}}(\lambda_{\text{CL}} - \lambda_0)}{\sqrt{\pi t}}A \quad [4]$$

Besides membrane absorption, water vapor can also be transported from the CL to the GDL and may desublimate inside the GDL due to the temperature gradient along the through-plane direction. However, water transported from the CL to GDL is limited by the low vapor saturation pressure below freezing and, consequently, ice formation in GDL is neglected in this model. Thus, the water vapor being transported to the GDL from CL is equal to the water removed through the outflow; i.e.

$$\dot{n}_{\text{GDL}}^{\text{H}_2\text{O}} = \dot{n}_{\text{outflow}}^{\text{H}_2\text{O}} \quad [5]$$

Under subzero temperatures, the maximum rate of water removed through the cathode exhaust can be obtained by assuming the outflow is always saturated such that

$$\dot{n}_{\text{outflow}}^{\text{H}_2\text{O}} = \zeta_c\frac{IA}{4F}\frac{1}{0.21}\frac{p_{\text{sat}}^{\text{H}_2\text{O}}}{p_c} \quad [6]$$

where the Goff Gratch equation[12] is employed for the saturation pressure of water vapor over ice, $p_{\text{sat}}^{\text{H}_2\text{O}}$. Due to the low saturation pressure at low temperature, the water vapor escape through the exhaust is quite small compared with the water production rate from ORR. Figure 2 shows a comparison of the water removal rate at the exhaust with the water production rate for a PEFC discharging at 100 mA/cm^2. A stoichiometry of 2 has been used for the air cathode. If pure oxygen is used, the water removal rate would be about 5 times smaller than air. As can be seen, the water removal rate from the cathode outlet is much smaller than the water production rate, especially below freezing. Therefore, it is impossible to remove all the product water through the outflow during subzero startup.

From Eq. 1, 2, 4, and 5, the rate of water accumulation in the CL can be obtained. However, ice does not precipitate in pores until the gas in CL becomes saturated. Before this point, t_0, the water accumulated in CL is absorbed in the ionomers within CL. That is

$$\int_0^{t_0} \dot{n}_{\text{acc}}^{\text{H}_2\text{O}}dt = \frac{\rho_{\text{dry}}(\lambda_{\text{sat}} - \lambda_0)}{\text{EW}}\varepsilon_e\delta_{\text{CL}}A \quad [7]$$

Physically the right-hand side of Eq. 7 represents the water storage capacity of the ionomers in the cathode CL. For a 10 μm thick CL

with the ionomer content of 25% and initial water content of 4.0, this storage capacity is calculated to be 0.083 mg/cm^2. After t_0 or water saturation is reached in the CL, ice will precipitate at the rate of water accumulation. Defining the ice fraction as the volume fraction of the ice in CL pores to the total void space such that

$$s = \frac{V_{\text{ice}}}{V_{\text{void}}} \quad [8]$$

and assuming homogeneous ice formation, the ice fraction in the CL can thus be calculated from

$$s = s_0 + \int_{t_0}^{t} \frac{\dot{n}_{\text{acc}}^{\text{H}_2\text{O}} v_{\text{ice}}}{\varepsilon_{\text{CL}} \delta_{\text{CL}} A} dt = s_0 + \int_{t_0}^{t} \frac{(\dot{n}_{\text{CL}}^{\text{H}_2\text{O}} - \dot{n}_{\text{mem}}^{\text{H}_2\text{O}} - \dot{n}_{\text{GDL}}^{\text{H}_2\text{O}}) v_{\text{ice}}}{\varepsilon_{\text{CL}} \delta_{\text{CL}} A} dt \quad [9]$$

where s_0 is the initial ice fraction prior to cold start and v_{ice} the molar volume of ice. When the fuel cell temperature reaches the freezing point, ice starts to melt in the CL, absorbing latent heat of melting, which will be discussed shortly.

Heat balance.— To ensure a successful self-start, the fuel cell should raise its temperature beyond the freezing point before being shut down by ice in the CL. The duration a PEFC can operate is determined by the rate of ice filling the CL pores and the thermal capacity of the cell.

Self-startup depends on the waste heat produced from ORR while water is created. The waste heat produced in a PEFC can be subdivided into reversible heat and irreversible heat.[13] During cold start there is also heat released during phase transition of water

$$\dot{Q}_{\text{total}} = \dot{Q}_{\text{rev}} + \dot{Q}_{\text{irrev}} + \dot{Q}_{\text{phase}} \quad [10]$$

Consider a H_2/air fuel cell operated at temperature T, pressure P, and current density I on an electrode of surface area, A. The reversible heat, Q_{rev}, can be written as

$$\dot{Q}_{\text{rev}} = (-T\Delta S)\frac{I}{2F}A = \left(-T\frac{\partial U_o}{\partial T}\right)IA \quad [11]$$

where ΔS represents the entropy change of the overall reaction, and U_o is the equilibrium potential of the H_2/O_2 reaction with all reactants and products in gas phase, as expressed by

$$U_o = 1.23 - 9.0 \times 10^{-4}(T - 298.15) \quad [12]$$

In addition, the irreversible heat generation due to the cell operated at a lower voltage, U_{cell}, than the equilibrium U_o is simply given by

$$\dot{Q}_{\text{irrev}} = \left(-\frac{\Delta G}{2F} - U_{\text{cell}}\right)IA = (U_o - U_{\text{cell}})IA \quad [13]$$

where ΔG is the free-energy change of the H_2/O_2 reaction and the cell voltage U_{cell} can be calculated from Eq. 25. The irreversible heat is due to the electrochemical reactions and ohmic resistances.

In cold start, another heat source comes from phase transition of water, releasing heat during desublimation and absorbing heat during ice melting. That is

$$\dot{Q}_{\text{sg}} = \dot{n}_{\text{ice}}^{\text{H}_2\text{O}} h_{\text{sg}} \quad [14]$$

where h_{sg} is the latent heat of phase change between solid and vapor and $\dot{n}_{\text{ice}}^{\text{H}_2\text{O}}$ is the desublimation-melting rate.

Combining Eq. 10, 11, 13, and 14, the total heat generation, $\dot{Q}_{\text{total}}$, is thus given by

$$\dot{Q}_{\text{total}} = \left(U_o + \frac{h_{\text{sg}}}{2F} - T\frac{\partial U_o}{\partial T}\right)IA - U_{\text{cell}}IA \quad [15]$$

The sum of the first two terms in the brackets, $[U_o + (h_{\text{sg}}/2F)]$, physically denotes the thermal potential of the H_2/O_2 reaction with production water being ice. The last term in Eq. 15 represents the actual electrical energy produced by a fuel cell.

Heat losses from the cell to the surrounding $\dot{Q}_{\text{loss}}$ include those through the outflow and from bipolar plates and cell edges, which can be generally expressed as

$$\dot{Q}_{\text{loss}} = (\dot{m}C_p)_{\text{outlet}}T - (\dot{m}C_p)_{\text{inlet}}T_0 + h_o A(T - T_0) \quad [16]$$

When a cell is thin and the end effects are negligible, spatially uniform temperature is a good approximation. By applying the energy balance over the entire cell with the assumption of spatially uniform temperature, the temperature of a PEFC during cold start can be calculated from

$$(mC_p)_{\text{cell}}(T - T_0) = \int_0^t (\dot{Q}_{\text{total}} - \dot{Q}_{\text{loss}})dt \quad [17]$$

where the left side refers to the sensible heat of all cell components.

Voltage losses in the presence of ice formation.— The effect of ice formation on the CL electrochemical performance is similar to that of flooding. Ice hinders oxygen transport and reduces the active catalytic sites. The difference between the freezing problem and the flooding problem is that liquid water can be continually transported out of the cathode CL and a steady-state solution exists for the flooding problem, while in the freezing problem, the ice precipitated inside the CL pores cannot be removed; thus, the PEFC cold start is an inherently transient problem.

The blockage of oxygen diffusion can be described by the effective diffusion coefficient D^{eff} with a decreasing effective porosity[14]

$$D^{\text{eff}} = D^{\text{O}_2}[\varepsilon_{\text{CL}}(1 - s)]^{1.5} \quad [18]$$

where D is the diffusion coefficient of oxygen in air and ε_{CL} the CL porosity. The same hindrance for oxygen applies to water vapor through the CL, further promoting ice formation.

The surface coverage effect in the presence of ice can be expressed via a decreasing ECA. That is

$$a^{\text{eff}} = a(1 - s)^n \quad [19]$$

In the present work, a linear relationship (i.e., $n = 1$) is assumed between the fraction of surface coverage and the ice volume fraction. In reality, this relationship depends strongly on the microscale morphology of ice formed in the CL. If a sheetlike shape is formed, the surface could be totally covered by a small volume fraction of ice, thereby rendering n to be very large. If the ice morphology is needlelike, the exponent becomes exceedingly small. Experimental work is ongoing in our laboratory to determine n in Eq. 19.

Electrochemical kinetics can be described by Tafel kinetics, i.e.

$$j = ai_0(1 - s)\frac{c_{\text{CL}}^{\text{O}_2}}{c_{\text{ref}}^{\text{O}_2}} \exp\left(-\frac{RT}{\alpha_c F}\eta_c\right) \quad [20]$$

Based on the experimental data of Parthasarathy et al.,[15] the temperature dependence of the ORR kinetic parameter is approximated as

$$i_0(T) = i_0(353.15\text{ K})\exp\left[-11{,}000\left(\frac{1}{T} - \frac{1}{353.15}\right)\right] \quad [21]$$

This correlation developed for the temperature range above freezing is, nevertheless, extended to cell temperatures below freezing in the present work. Clearly, ORR becomes more sluggish with decreasing temperature.

The consumption rate of oxygen is proportional to the current density. Under the assumption that the reaction current is uniform throughout the CL, the oxygen concentration follows a quadratic distribution along the CL thickness, as governed by

$$\frac{\partial}{\partial x}\left(D^{\text{O}_2}[\varepsilon_{\text{CL}}(1 - s)]^{1.5}\frac{\partial c_{\text{CL}}^{\text{O}_2}}{\partial x}\right) = \frac{j}{4F} = \frac{I}{4F\delta_{\text{CL}}} \quad [22]$$

where $x = 0$ denotes the CL/membrane interface and $x = \delta_{\text{CL}}$ the CL/GDL interface. Solving Eq. 22 analytically, one can obtain the

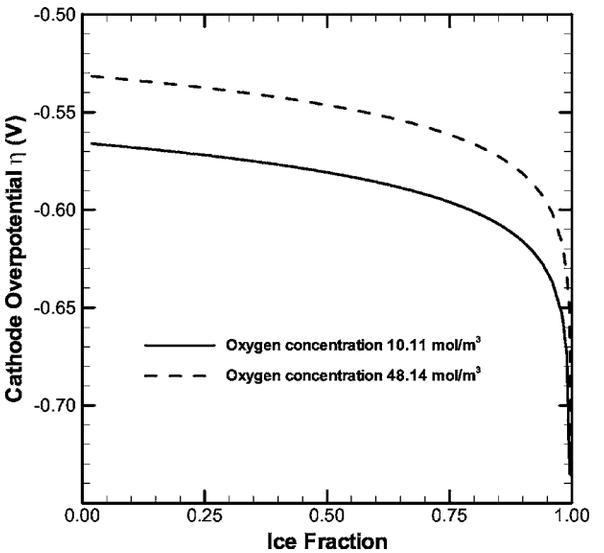

Figure 3. Effects of ice formation on cathode overpotential.

local concentration of oxygen in CL as a function of that in the flow channel. That is

$$c_{\mathrm{CL}}^{\mathrm{O_2}} = c_C^{\mathrm{O_2}} - \frac{I}{4F}\left(\frac{\delta_{\mathrm{GDL}}}{D^{\mathrm{O_2}}\varepsilon_{\mathrm{GDL}}^{1.5}}\right) - \frac{I}{4F}\frac{\delta_{\mathrm{CL}}\left[1-\left(\frac{x}{\delta_{\mathrm{CL}}}\right)^2\right]}{D^{\mathrm{O_2}}[\varepsilon_{\mathrm{CL}}(1-s)]^{1.5}} \quad [23]$$

Taking the average of the oxygen concentration in the cathode CL and substituting it into Eq. 20, one can obtain the cathode overpotential as a function of the current density and the ice fraction in the cathode CL. That is

$$\eta_c = -\frac{RT}{\alpha_c F}\ln\left(\frac{I}{(1-s)ai_0\delta_{\mathrm{CL}}} \cdot \frac{c_{\mathrm{ref}}^{\mathrm{O_2}}}{c_C^{\mathrm{O_2}} - \frac{I}{4F}\left(\frac{\delta_{\mathrm{GDL}}}{D^{\mathrm{O_2}}\varepsilon_{\mathrm{GDL}}^{1.5}} + \frac{2\delta_{\mathrm{CL}}}{3D^{\mathrm{O_2}}[\varepsilon_{\mathrm{CL}}(1-s)]^{1.5}}\right)}\right) \quad [24]$$

where the two terms related to $(1-s)$ represent the two effects of ice formation, i.e., the reduction in ECA and the hindering of oxygen transport.

The effect of ice formation on the cathode ORR overpotential is plotted in Fig. 3 for pure oxygen and air, respectively, for a PEFC operated at 100 mA/cm^2 under −20°C. The mass transport loss does not become severe until the ice fraction reaches 0.9. This is due to the small current density commonly involved in cold start. Also, the difference between using air (10.11 mol/m^3) and pure oxygen (48.14 mol/m^3) is small, implying that using pure oxygen is of minimal help for the cold start application. At high ice fractions (>0.9), the cathode overpotential increases sharply due to both reduction in ECA and blockage of oxygen transport. As a consequence, the fuel cell voltage will rapidly drop.

Cell voltage can be estimated by subtracting the activation loss and ohmic loss from the equilibrium potential. That is

$$U_{\mathrm{cell}} = U_o - \eta_a + \eta_c - IR_\Omega \quad [25]$$

The anode overpotential due to hydrogen oxidation can be safely ignored. The ohmic loss comes from the protonic resistance of the electrolyte in both membrane and CL, the contact resistance, and the electronic resistances of the CL, GDL, and bipolar plates. Note that the contact resistance and electronic resistances are small and thereby neglected here. The protonic resistance in the anode CL is also negligible because HOR occurs primarily at the CL/membrane interface. Assuming the ORR reaction occurs uniformly in the cathode CL, the ohmic loss can thus be calculated by

$$IR = I\left(\frac{\delta_{\mathrm{mem}}}{\kappa_{\mathrm{mem}}} + \frac{\delta_{\mathrm{CCL}}}{2\kappa_{\mathrm{CCL}}\varepsilon_e^{1.5}}\right) \quad [26]$$

where κ_{mem} and κ_{CCL} are the proton conductivities evaluated at different water contents in the membrane and CL, respectively.

A complete solution of cold start problem.— The PEFC cold start problem can be fully described by three interacting processes: ice formation based on water balance; temperature rise based on energy balance; and cell voltage drop-down as a function of ice formation. Ice formed blocks oxygen transport from the gas channel to the reaction sites and partially covers the ECA with ice sheets. Simultaneously, heat production from ORR raises the cell temperature, which in return alters the ice formation. These coupled phenomena have been considered in the present model by assuming a spatially uniform temperature and homogeneous ice formation in the CL.

A typical cold start process can be divided into four distinct stages.

1. *Stage 1.* The fuel cell starts up and water is produced at the cathode to raise the water vapor concentration in the gas until saturation. No ice precipitation occurs in CL. This stage is characterized by t_0 as calculated from Eq. 7.

2. *Stage 2.* Once water saturation is reached in the gas phase in CL, further product water will precipitate in the CL as ice. At the same time, the waste heat produced will warm up the fuel cell. There are two scenarios in this stage. If the cell temperature is still below freezing before the CL is filled up with ice, i.e., the ice fraction reaches unity, the fuel cell is shut down, marking the end of this second stage or cold start. The shutdown time can be estimated by

$$\int_{t_0}^{t_{\mathrm{shutdown}}} \dot{n}_{\mathrm{acc}}^{\mathrm{H_2O}}\,dt = \frac{\varepsilon_{\mathrm{CL}}\delta_{\mathrm{CL}}}{v_{\mathrm{ice}}}(1-s_o) \quad [27]$$

Otherwise, time needed to raise fuel cell temperature to the freezing point can be calculated by solving the energy balance, that is, $T(t_1) = T_{\mathrm{freeze}}$. At this point, the ice fraction reaches its maximum value $s(t_1)$. To achieve successful self-startup, t_1 should always be less than t_{shutdown}. The cell temperature and ice fraction evolution can be calculated by solving the energy and water balance equations coupled with the cell voltage expression given in Eq. 25.

3. *Stage 3.* If the cell temperature successfully rises to the freezing point before the CL is shut down by ice, the ice in the CL starts to melt, absorbing the waste heat produced from the cell and keeping the cell temperature constant at the freezing point until all ice vanishes, i.e., $s(t_2) = 0$. During ice melting, the cell temperature remains constant at the freezing point, i.e., $T = T_{\mathrm{freeze}}$, and the ice melting rate can be calculated from the energy balance. That is

$$s = s(t_1) + \int_{t_1}^{t} \frac{-(\dot{Q}_{\mathrm{rev}} + \dot{Q}_{\mathrm{irrev}} - \dot{Q}_{\mathrm{loss}})v_{\mathrm{ice}}}{\varepsilon_{\mathrm{CL}}V_{\mathrm{CL}}h_{\mathrm{sg}}}dt \quad [28]$$

4. *Stage 4.* When all ice melts in the CL, the cell temperature rises further to a normal operating temperature, at which point cell cooling must be initiated to maintain steady operation. The cell temperature can be determined by Eq. 17 in this stage.

Results and Discussion

The analytical model presented in the preceding section is used to study and understand the physics governing PEFC cold start. Calculations are carried out to assess effects of the startup temperature, the initial water content in the membrane, and the thermal mass of bipolar plates. In these simulations, both anode and cathode gas flow rates correspond to a stoichiometric flow ratio of 2 at the cur-

Table I. Cell parameters.

Description	Unit	Value
Cell configuration		
Anode/cathode bipolar plate thickness	m	1.0×10^{-3} 0.5×10^{-3} 1.5×10^{-3}
Anode/cathode GDL thickness	m	3.0×10^{-4}
Anode/cathode CL thickness	m	1.0×10^{-5}
Membrane thickness, Nafion 112	m	5.1×10^{-4}
Anode/cathode GDL porosity		0.6
Anode/cathode CL porosity		0.5
Volume fraction of ionomers in CL		0.2
Equivalent weight of membrane, Nafion 112	kg/mol	1.1
Dry density of membrane, Nafion 112	kg/m^3	1.98×10^3
Electrochemical kinetics		
Anode reference exchange current density, 353.15 K	A/m^2	1.0×10^9
Cathode reference exchange current density, 353.15 K	A/m^2	1.0×10^4
Anode transfer coefficient		2
Cathode transfer coefficient		1
Faraday constant	C/mol	96,487
Transport parameters		
H_2O diffusivity in membrane	m^2/s	1.0×10^{-12}
Membrane proton conductivity	S/m	1.0
Electro-osmotic drag coefficient		0.5
Thermal properties		
Anode/cathode GDL heat capacity	$J/K\ m^3$	5.68×10^5
Anode/cathode catalyst layer heat capacity	$J/K\ m^3$	1.69×10^6
Membrane heat capacity	$J/K\ m^3$	1.65×10^6
Anode/cathode bipolar plate heat capacity	$J/K\ m^3$	1.57×10^6
Latent heat of desublimation	J/mol	5.1×10^{-4}
Molar volume of ice	m^3/mol	2.0
Operating conditions		
Discharge current density	A/m^3	1000
Initial water content in membrane		3
Heat transfer coefficient between cell and surrounding	$W/K\ m^2$	50[a] 20
Startup temperature	K	253.15[a] 263.15

[a] Default value if not specified.

rent density of 100 mA/cm^2 and the inlet pressure of 1.0 atm. The cell parameters used in the calculations are listed in Table I, with the startup current density of 100 mA/cm^2 in all calculations.

The analytical solution of cold start with the startup temperature of −20°C is presented in Fig. 4. The initial water content in the membrane corresponds to a cell purged with gas of 50% relative humidity prior to cold start. Figure 4 shows the evolution of ice fraction in the cathode CL, cell temperature, and voltage, respectively. It is seen that the fuel cell temperature cannot rise above freezing before the ice fraction reaches unity, meaning that the fuel cell is shut down by ice formation in the CL. Indeed, cell voltage experiences a quick drop-down in the final stage. Specifically, there is no ice precipitation during the first 33 s of cold start, and cell voltage experiences an increase due to membrane hydration by product water, and hence lowered protonic resistance. When ice forms inside the CL, the activation loss increases due to the oxygen blockage and ECA reduction, as shown in Fig. 3. However, when the ice fraction is still low, the cell voltage is increasing due to the improvement in membrane proton conductivity with more water uptake and faster ORR kinetics with rising cell temperature. The effect of ice formation becomes severe only when the ice fraction approaches unity, as characterized by the sharp drop in cell voltage.

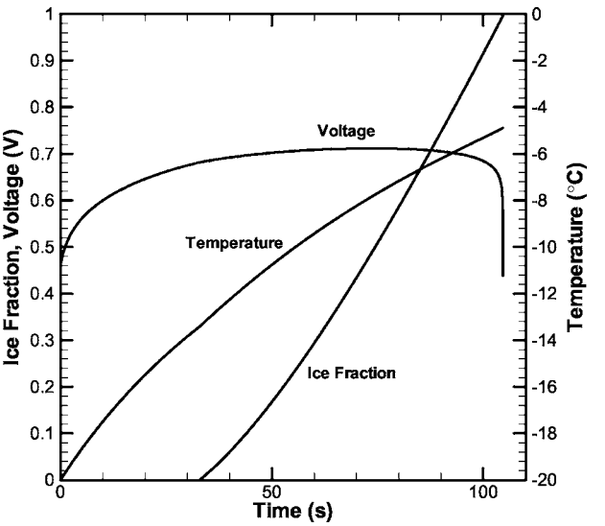

Figure 4. Evolution of ice fraction, cell temperature, and voltage during cold start from −20°C.

Figure 5 depicts the water fluxes in and out of the cathode CL during cold start, where a positive value indicates water accumulation and a negative represents water removal from the cathode CL. The water produced from ORR, together with the water dragged from the anode, can be either transported into the membrane and GDL, or freezes inside the CL. It is apparent from Fig. 5 that the outflow can only remove a negligibly small amount of water due to the combination of small flow rate and low vapor saturation pressure at −20°C. In the first 33 s, the product water is primarily absorbed by ionomers in CL. The increasing water content in the CL leads to a large water flux into the membrane. Once the water content in the catalyst layer reaches the maximum (i.e., equilibrium with saturated water vapor), the water flux into the membrane begins to decrease, as can be seen from the similar solution given in Eq. 4. Thereafter, ice formation inside the CL begins. At ~105 s, the catalyst layer is filled completely with ice and the fuel cell is shut down by ice clogging.

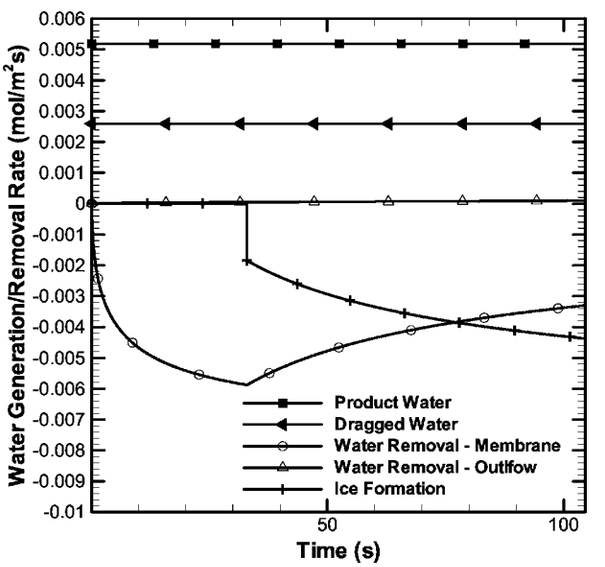

Figure 5. Water balance during cold start from −20°C.

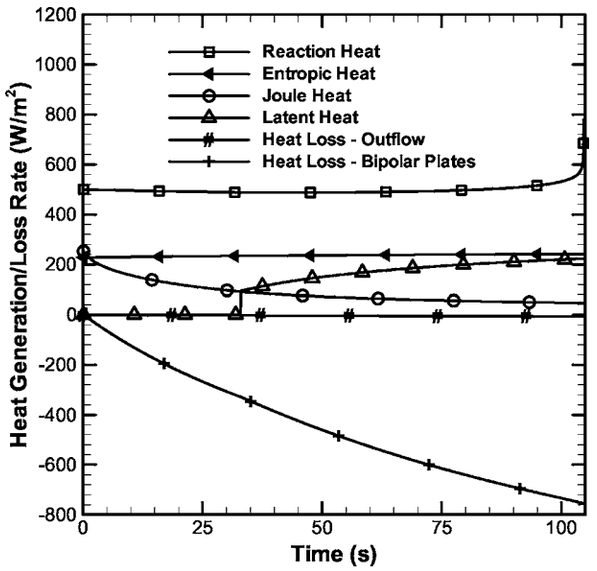

Figure 6. Breakdown of heat generation during cold start from −20°C.

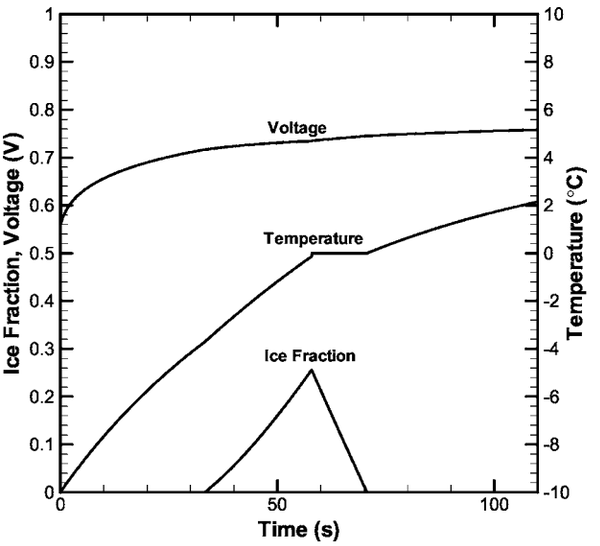

Figure 7. Evolution of ice fraction, cell temperature, and voltage during cold start from −10°C.

The breakdown of heat generation during this cold start is plotted in Fig. 6, where a positive value means a heat source and a negative value is a heat loss. The sensible heat, i.e., the heat warming the fuel cell, is the difference between the total heat generation and the heat loss. The reaction heat and entropic heat accounts for ~50 and 25% of the total heat generation, respectively. The Joule heat is large initially due to the large protonic resistance of the membrane, but decreases upon further discharge as more product water is absorbed by ionomers. After 33 s, there is latent heat released from water desublimation. At the end of discharge, the reaction heat, proportional to the cathode overpotential, increases dramatically due to the CL filling up with ice and resultant mass transport loss. The heat losses, both from the bipolar plates and through exhaust gases, are directly proportional to the temperature difference between the fuel cell and the surroundings. The waste heat brought out by the outflow is negligibly small in the entire duration of startup.

The startup from −20°C is unsuccessful because the temperature cannot reach the freezing point before the cathode CL is filled up with ice. Increasing the startup temperature is more likely to achieve a successful startup, which reduces not only the heat loss to the environment but also the heat required for the fuel cell to reach the freezing point. As shown in Fig. 7-9, a PEFC start is studied by the analytical model with the same configuration and conditions except that the ambient temperature is −10°C. In Fig. 7, the cold start process can be clearly divided into four stages: (*i*) in the first 33 s, water vapor builds up in the CL until the gas phase becomes saturated; (*ii*) ice starts to form and reaches its peak volume fraction at 58 s when the cell temperature rises to the freezing point; (*iii*) the formed ice starts to melt and the temperature remains at the freezing point; and (*iv*) once the ice completely melts, the temperature rises again toward the designated operating point. The temperature increase below freezing is faster than that above freezing due to the latent heat released from ice formation and increased heat loss to the environment when the cell temperature is higher. Figure 7 also shows that the cell voltage rises during the startup from −10°C, which is mainly due to the membrane resistance reduction and fast kinetics with a rising temperature. However, between 33 and 58 s, the voltage rise slows down due to ice formation. The characteristics of water flow during cold start as displayed in Fig. 8 are similar to the −20°C case except that during ice thawing, the ice melted joins the water generation in CL, thereby increasing the required rate of water removal. The breakdown of heat generation is given in Fig. 9. The most noticeable difference from the −20°C case is that during thawing there is heat absorbed by phase change. In addition, the heat loss from bipolar plates is seen to decrease with time or increasing cell temperature and levels once the cell temperature stays at the freezing point.

It is of interest to understand the dependence of PEFC cold start performance on initial water distribution, particularly the initial water content in the membrane as effected by gas purge. It is clear from the above discussions that the membrane plays a pivotal role in storing the product water from the CL. Therefore, the initial membrane water content is an important measure of the fuel cell initial condition prior to cold start. In practice, a uniform initial water content λ_0 can be realized by using a purge gas of certain relative humidity (RH) to purge the fuel cell for an extended time, say several hours. In so doing, the membrane λ_0 reaches thermodynamic equilibrium with the RH of purge gas. The difference between this initial water content and the maximum value corresponding to a fully hydrated membrane (i.e., λ_{sat}) then defines the potential of water uptake in the membrane during cold start, i.e., $\Delta\lambda = (\lambda_{sat}$

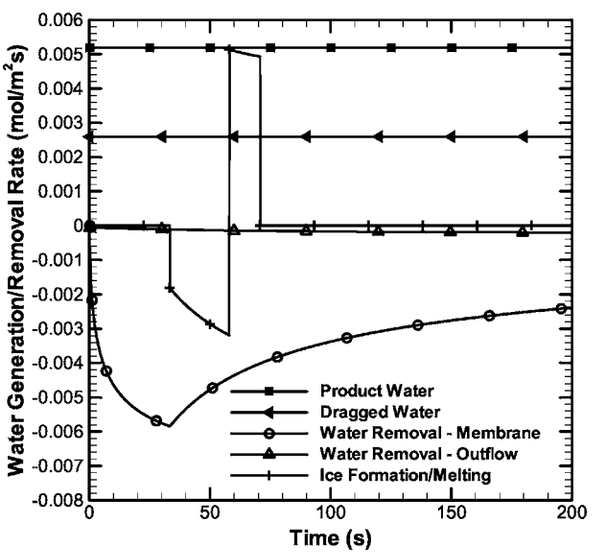

Figure 8. Water balance during cold start from −10°C.

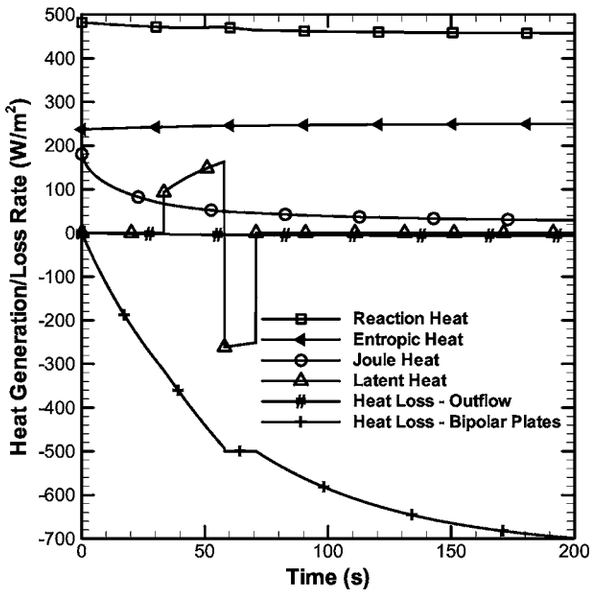

Figure 9. Breakdown of heat generation during cold start from −10°C.

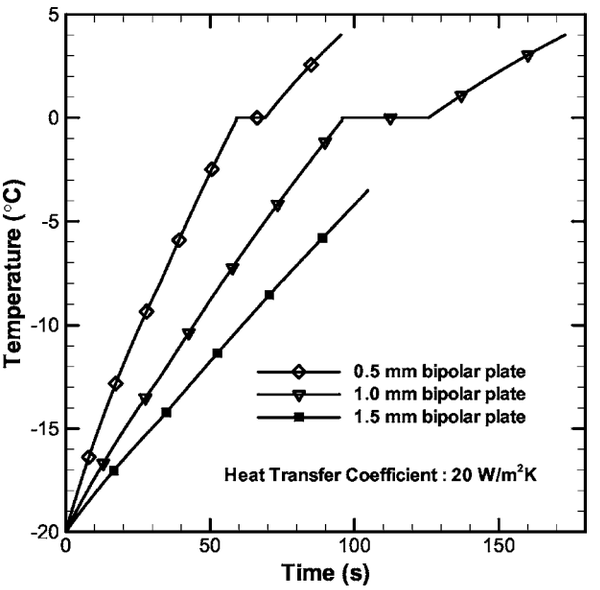

Figure 11. Effects of thermal mass of bipolar plates on cold start from −20°C.

$-\lambda_0$). To quantify cold start performance, we choose the cumulative product water in mg/cm^2 because the product water combines the effects of current density and operational time and directly correlates with the total amount of heat produced. Higher product water indicates more heat produced and hence better cold start performance. The product water achievable before shutdown for startups at −20°C with varying initial membrane water content is displayed in Fig. 10. It is clearly shown that the initial water condition has an important impact on cold start. When the membrane is fully hydrated prior to cold start, the water uptake potential is zero and no water can be stored in the membrane during cold start. This leads to the minimum product water cumulative before cell shutdown. With increasing water uptake potential in the membrane, product water (and heat) increases significantly as some can be stored in a partially dry membrane. Further, the increase in product water is nonlinear, as evident from the comparison with a linear relation, also shown in Fig. 10 as the dashed line, indicating that a partially dry membrane not only enhances the water flux into the membrane, but also gains more time for water removal from the CL.

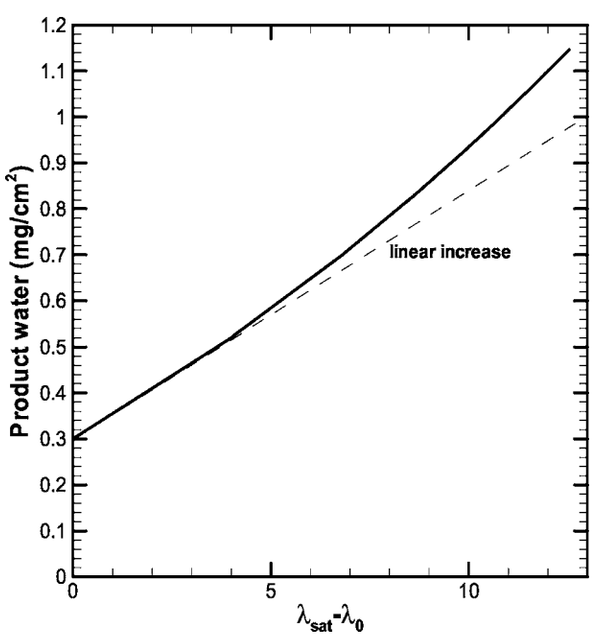

Figure 10. Effects of initial water content in the membrane on cold start from −20°C.

Finally, reducing the thermal mass of a fuel cell, particularly its bipolar plates, will improve cold start by raising the cell temperature more quickly for a given amount of heat generated from ORR. To quantify this effect, the −20°C startup of fuel cells with graphite bipolar plates of thickness 0.5, 1, and 1.5 mm, respectively, is analyzed using the present model, under otherwise identical conditions. A constant heat transfer coefficient of 20 W/m^2 K is chosen to simulate the heat loss from the bipolar plates to the surroundings. Figure 11 depicts the temperature evolution curves in the three cases. It is seen that fuel cells with less thermal mass, or thinner bipolar plates, can start up successfully. For the fuel cell with 1.5 mm graphite bipolar plates, the temperature cannot break through the freezing point from −20°C before the CL is filled up with ice; therefore, startup of this fuel cell fails. Comparing the temperature curves for 0.5 and 1.0 mm bipolar plates, it is seen that the time needed to melt all ice is shorter with less thermal mass because the amount of ice formed is smaller. Furthermore, the heat loss to the surroundings is also an important factor when comparing the thermal curve of 1.0 mm bipolar plates with Fig. 4, where a larger heat transfer coefficient of 50 W/m^2 K is employed and the startup fails. This means that proper thermal insulation can also improve cold start performance of a PEFC. In a stack environment, the heat transfer coefficient h_o represents the cell-to-cell heat loss. Therefore, end cells featuring higher h_o are more difficult to start, where cells in the middle of a stack, as characterized by smaller h_o, are much easier to start.

Conclusions

PEFC cold start is physically controlled by intricately coupled water and heat transport. If production water from ORR cannot be sufficiently removed and if waste heat generated is insufficient to raise the cell temperature up to the freezing point, ice formation occurs in the cathode CL, thereby causing voltage drop-down and even shutdown of the fuel cell. The single criterion of a successful startup is that the cell temperature rises above freezing before the

cathode CL is completely filled with ice. In the delicate balance of water and heat generation, the ionomeric membrane plays an important role as it can divert water from the CL and hence buys time for the fuel cell to operate longer and generate more heat for warm-up.

An analytical model of PEFC cold start has been developed in this work and applied to study the effects of the startup temperature, initial water content of membrane, and thermal mass of the fuel cell. For a higher startup temperature, the energy required to heat up the fuel cell to the freezing point is lower, and also the heat loss to the environment is less due to a small temperature difference. Consequently, there is a higher likelihood of self-startup. A dryer membrane initially having higher water uptake potential, gives rise to better cold start performance as it not only increases the water absorbed in the membrane, but also offers more time for water to be removed from the cathode CL by other means. For this reason, gas purge is considered as an essential part of cold start operation. Finally, reducing thermal mass of bipolar plates and applying proper thermal insulation can also lead to a quicker temperature rise with the same amount of waste heat released, thereby increasing the chance for a successful startup.

Experimental validation of this analytical model as well as a three-dimensional multiphase model to accommodate additional physical phenomena involved in PEFC cold start and temperature dependency of key materials properties is presented in a separate publication.

Acknowledgments

Financial support of this work was provided in part by Penn State Materials Research Institute and ECEC industrial sponsors.

The Pennsylvania State University assisted in meeting the publication costs of this article.

List of Symbols

a	active catalyst area per unit volume, L/m
A	projection of the reaction area, A^2
c^i	molar concentration of species i, mol/m^3
C_p	thermal capacity, J/kg K
D^i	mass diffusivity of species i, m^2/s
EW	equivalent weight of polymer membrane, kg/mol
F	Faraday's constant, 96,487 C/mol
G	Gibbs free energy, J
h_o	heat transfer coefficient between cell and external, W/K m^2
h_{sg}	enthalpy change between ice and water vapor, J/mol
i_o	reference exchange current density, A/m^2
I	current density, A/cm^2
j	transfer current density, A/m^3
m	mass, kg
$\dot{m}$	mass flow rate, kg/s
n^{H_2O}	water storage capacity, mol
$\dot{n}^{H_2O}$	water generation/removal rate, mol/s
n_d	electro-osmotic drag coefficient
p	pressure, Pa
$\dot{Q}$	heat generation/loss rate, mol/s
R	universal gas constant, 8.314 J/mol K
R_Ω	ohmic resistance, Ω
s	ice fraction
S	entropy, J/K mol
t	time, s
T	temperature, K
U_o	reference open circuit potential, V
U_{cell}	cell voltage, V
v_{ice}	specific volume of ice, m^3/mol
V	volume, m^3

Greek

α	transfer coefficient
η	overpotential, V
ε	porosity
ε_e	volume fraction of ionomers in catalyst layer
κ	ionic conductivity, S/m
λ	water content in ionomer, # H_2O/SO_3^-
ρ	density, kg/m^3
δ	thickness, m
ζ	stoichiometry coefficient of the reactant

Subscripts

0	initial condition
a	anode
c	cathode
CL	catalyst layer
GDL	gas diffusion layer
mem	membrane
ref	reference
sat	saturation

Superscripts

O_2	oxygen
H_2O	water
H_2	hydrogen
eff	effective

References

1. R. C. McDonald, C. K. Mittelsteadt, and E. L. Thompson, *Fuel Cells*, **4**, 208 (2004).
2. E. Cho, J. J. Ko, H. Y. Ha, S. A. Hong, K. Y. Lee, T. W. Lim, and I. H. Oh, *J. Electrochem. Soc.*, **150**, A1667 (2003).
3. E. Cho, J. J. Ko, H. Y. Ha, S. A. Hong, K. Y. Lee, T. W. Lim, and I. H. Oh, *J. Electrochem. Soc.*, **151**, A661 (2004).
4. M. Oszcipok, D. Riemann, U. Kronenwett, M. Kreideweis, and M. Zedda, *J. Power Sources*, **145**, 407 (2005).
5. M. Oszcipok, M. Zedda, D. Riemann, and D. Geckeler, *J. Power Sources*, **154**, 404 (2006).
6. K. Weisbrod, J. Hedstrom, J. Tafoya, R. Borup, and M. Inbody, in *Proceedings of Fuel Cell Seminar 2000*.
7. M. Sundaresan, Ph.D. Thesis, University of California, Davis (2004).
8. Y. Hishinuma, T. Chikahisa, F. Kagami, and T. Ogawa, *JSME Int. J., Ser. B*, **47**, 235 (2004).
9. T. E. Springer, T. A. Zawodzinski, and S. Gottesfeld, *J. Electrochem. Soc.*, **138**, 2334 (1991).
10. T. E. Springer, M. S. Wilson, and S. Gottesfeld, *J. Electrochem. Soc.*, **140**, 3513 (1993).
11. H. S. Carslaw and J. C. Jaeger, *Conduction of Heat in Solids*, 2nd ed., Oxford Science Publications, Oxford (1986).
12. Smithsonian Meteorological Tables, 5th ed., p. 350 (1984).
13. H. Ju, H. Meng, and C. Y. Wang, *Int. J. Heat Mass Transfer*, **48**, 1303 (2005).
14. R. E. Meredith and C. W. Tobias, in *Advances in Electrochemistry and Electrochemical Engineering 2*, C. W. Tobias, Editor, Interscience Publishers, New York (1962).
15. A. Parthasarathy, S. Srinivasan, A. J. Appleby, and C. R. Martin, *J. Electrochem. Soc.*, **139**, 2530 (1992).